pp. 1–13 (2024)

Patient specific numerical hemodynamics for postoperative risk assessment: series case study of EC-IC cerebral bypass

Iu. Kuianova*[a], A. Bervitskiy[bc], A. Dubovoy[b], and D. Parshin [a]

Abstract — The study is devoted to the hemodynamics during cerebral vascular bypass surgery for the treatment of cerebral aneurysms in two patients. The location, morphological characteristics and treatment approaches of the patients were similar, but different outcomes were observed as a result of the performed microsurgical procedures . Computational approach was used to analyze the hemodynamic differences of aneurysms, treated via extra-intra cranial (EC-IC) cerebral bypass shunt. The paper presents a new criterion based on the energy parameters of healthy compartment of cerebral circulation. The applied approach demonstrates a new effective method of preoperative risk modelling for medical decision-making.

Keywords: Cerebral shunt, risk criterion, cerebral aneurysm, bypass patency, fluid-structure interaction problem, patient specific domain

MSC 2010: 76Z05,92C55,76M12,74B05,65M08,35B30

Treatment of the intracranial aneurysms (IA) is one of the most challenging problems in neurosurgery [7]. IA present in 2 out of 100 people [14]. Rupture of IA, leads to an intracranial hemorrhage with severe consequences: neurological deficit, disability and death [24, 31].

Possible treatment options include endovascular treatment [4, 11, 23] and microsurgery clipping [5, 10, 26]. In some cases, none of the methods is able to achieve occlusion of the aneurysm itself, in which case it is necessary to occlude the parent artery. In this case, to avoid cerebral ischemia, it is necessary to form a vascular anastomosis, namely bypass. It should be noted that the formation of a bypass significantly changes the geometry of the cerebral vessels, which leads to a redistribution of cerebral blood flow. These changes do not always have a beneficial effect on cerebral hemodynamics. Thus, before surgery, it is necessary to evaluate all the associated risks. Currently, there are many works on the hemodynamics of cerebral vessels associated with bypasses [3, 12, 15, 25, 27, 37, 38]. However, almost every study is based on the consideration of one or more clinical cases, without the formation of common criteria and approaches for assessing preoperative risks. In some works, the authors propose general approaches [32] to assessing the effective-

[a]Lavrentyev Institute of Hydrodynamics, Novosibirsk 630090, Russia
* E-mail: kuianovaj@gmail.com
[b]Federal Neurosurgical Center, Novosibirsk 630048
[c]Novosibirsk State Medical University, Novosibirsk 630091
The study was supported by the Russian Science Foundation grant No. 20-71-10034.

ness of creating a bypass, however, such approaches are mainly based on primitive hydraulic models of local hemodynamics at the site of the shunt, without affecting the remaining vessels of the circle of Willis (COW) or use only local hemodynamic parameters like wall shear stress (WSS). Thus, the problem of assessing the risks of postoperative complications during the formation of cerebral bypass has not been fully elucidated. Meanwhile, the use of non-invasive methods for assessing cerebral blood flow [36], as well as performing model numerical calculations [17, 21, 29], makes it possible to formulate criteria for the effectiveness of anastomoses.

This paper presents an approach for calculating a new risk criterion based on the results of numerical simulations for CT angiography data of two patients who had similar morphology of the aneurysms and, at the same time, different postoperative outcomes.

1. Methods

1.1. Description of clinical cases and surgical intervention

Patient A was a 20 year-old male diagnosed with a giant cavernous IA portion of the left ICA. The patient underwent a craniotomy on the left, the creation of EC-IC [8, 20, 30] high-flow bypass between the left maxillary artery and the M1 segment of the left middle cerebral artery (MCA) using an arterial autograft.

Then the patient was transferred to the endovascular operating room and endovascular proximal occlusion of the aneurysm was performed using microcoils and adhesive composition. In the postoperative period, a right sided hemiparesis was noted.

Control cerebral angiography was performed: the shunt is patent, however, in a day after the treatment thrombosis of the proximal part M1 of the left MCA segment was noted.

Patient B was a 50 year-old female diagnosed with giant fusiform partially thrombosed aneurysm of the cavernous part of the right ICA saccular aneurysm of the V4 segment of the right VA. The patient underwent right-sided pterional craniotomy, the creation of EC-IC high-flow bypass between the temporal artery (TA) and the right MCA using the radial artery, proximal occlusion of the giant fusiform cavernous aneurysm of the right ICA. The postoperative period was uneventful.

1.2. 3D-geometry of the circle of Willis

To restore the patient-specific vessel geometry of the circle of Willis (COW) of both patients, we used computed tomography (CT) angiography data obtained on a Siemens Somatom Definition AS medical computer tomograph (64 slice-scanner). The extracted medical DICOM images were processed using the free software ITK SNAP [33] which is widely used to reconstruct the 3D geometry of vascular networks [6, 18, 35].

1.3. Gathering equations

We performed a numerical simulation of the blood flow in patient-specific 3D configurations of cerebral vessels. The calculations were performed for two real geometry cases (before and after surgery) and two virtual ones: so called an alternative technique (when only ICA occlusion without bypasses was done) and so called 'healthy network' (the cerebral aneurysm domain was virtually cut off from the COW geometry before the surgery). The calculations were performed in a stationary formulation with rigid walls, in an unsteady formulation with rigid walls (taking into account the pulsating nature of the blood flow: the flow profile is taken from [16]), as well as in a stationary FSI formulation (taking into account the elastic nature of the blood-wall interaction arteries).

In all formulations of the problem, the blood was assumed as a Newtonian fluid (with the density $\rho = 997$ kg/m^3 and viscosity $\mu = 0.0032$ Pa$\cdot$s), which means that the fluid viscosity does not depend on the shear rate [1]. We suppose that due to the fact that the rather high flow rates allow to use Newtonian fluid model and if the required criterion is qualitatively achieved for a model that is simpler and cheaper in terms of time cost, then it is this model that should be used. Otherwise, when the blood flow velocity is sufficiently low (for example, in processes involving the gradual occlusion of an aneurysm), non-Newtonian models, such as the Carreau–Yasuda, Casson models and some others [2, 22], will be more accurate to describe the processes occurring in the vascular system.

The problem was considered in three different formulations: a stationary flow (with rigid walls and the FSI model) and an unsteady flow with rigid walls. The governing equations for all formulations are given by the formulae:

$$\rho\left(\frac{\partial \mathbf{u}}{\partial t} + (\mathbf{u}\cdot\nabla)\mathbf{u}\right) = -\nabla p + \nabla\cdot\tau, \qquad \nabla\cdot\mathbf{u} = 0 \tag{1.1}$$

where $\mathbf{u}$ is the velocity field, t is time, p is pressure and τ is the deviatoric stress tensor, which can be written in the following way:

$$\tau_{ij} = \mu\dot{\gamma} \tag{1.2}$$

due to the Newtonian approach being used, where $\dot{\gamma}$ is a shear rate. The Hooke law of the mechanics of the cerebral aneurysm wall for FSI models is given by the formula:

$$F = k\Delta l \tag{1.3}$$

where k is the stiffness factor and Δl is the elongation.

1.4. Boundary conditions

On the vessel wall the no-slip condition takes place:

$$\mathbf{v} = 0, \quad \mathbf{x} \in \partial\Omega_{\text{wall}} \tag{1.4}$$

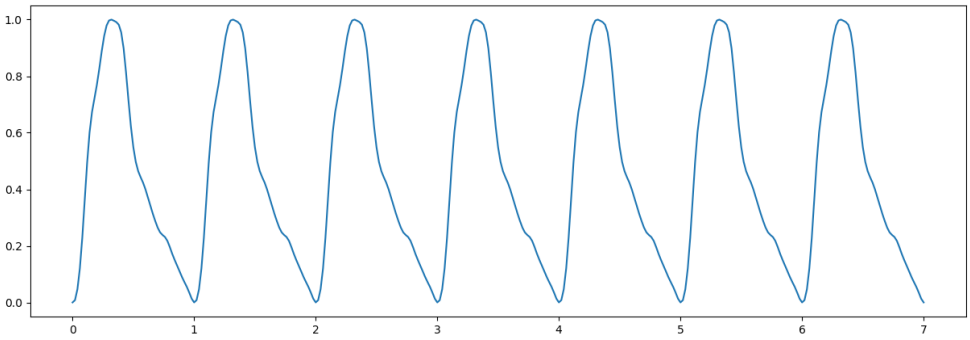

Figure 1. Normalized velocity profile measured in the ICA.

where $\partial\Omega_{\text{wall}}$ is the fluid domain surface. For stationary flow, the mass velocity of blood flow, normal for a healthy person, was used as boundary conditions at the inputs of the configurations [34]. The pressure corresponding to the average measurement data was set at the outputs. In the case of the unsteady flow we use the velocity profile for ICA blood flow in the norm, calculated on the basis of mass flow rates in the corresponding arteries (see Fig. 1). The normal velocity and the given pressure are specified at the inlets $\partial\Omega_{\text{in}}$ and the outlets $\partial\Omega_{\text{out}}$, respectively:

$$\begin{aligned} \mathbf{v} &= v_{\text{in}}(t)\mathbf{n}, \quad \mathbf{x} \in \partial\Omega_{\text{in}}, \quad t \in (0,T) \\ p &= p_{\text{out}}(t), \quad \mathbf{x} \in \partial\Omega_{\text{out}}, \quad t \in (0,T). \end{aligned} \tag{1.5}$$

In unsteady formulation the initial conditions are those as following:

$$\mathbf{v}|_{t=0} = 0, \quad p|_{t=0} = p_{\text{atm}}, \quad \mathbf{x} \in \Omega \tag{1.6}$$

where p_{atm} is the reference pressure, which is equal to atmospheric one (760 mmHg).

1.5. Meshing

In each case an unstructured tetrahedral mesh that is refined at bends was used. The number of mesh elements for each configuration was approximately 1.5 million. Considering the fact that blood is a viscous fluid, five prismatic layers were built along the wall.

The optimal amount of grid elements was found for the calculations. Calculations were carried out with 4 different grids, consisting of 1, 2, 4, and 8 million elements (grids M1-M4, respectively). To search for the optimal one among the specified grids, the values of mass flow rates at the outputs of the configuration were compared varying the number of elements (the outputs of the specified configuration are presented in Fig. 2).

Mass flow data for each of the grids is presented in Table 1. It is seen from Table 2, that as the number of grid elements increases, the difference in mass flow

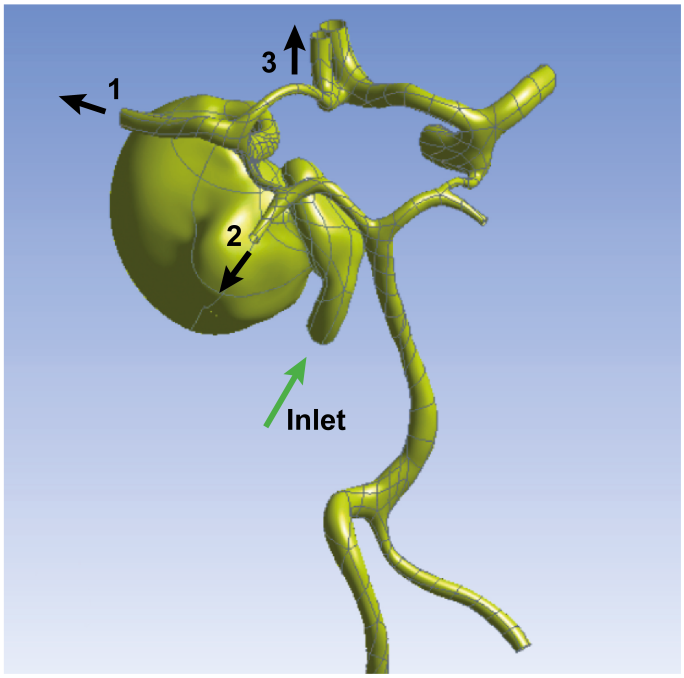

Figure 2. Arrows indicate the input and output from the configuration.

Table 1. Values of the mass flow at the outlets on M1-M4 grids.

Mass flow (g/s)	Mesh 1 (M1)	Mesh 2 (M2)	Mesh 3 (M3)	Mesh 4 (M4)
Outlet 1	2.606	2.611	2.61	2.61
Outlet 2	0.989	0.989	0.989	0.989
Outlet 3	1.405	1.4	1.401	1.405

Table 2. Difference in the mass flow on M1-M4 grids.

Difference in mass flow (g/s)	M1-M2	M2-M3	M3-M4
Outlet 1	−0.005	0.001	0
Outlet 2	0	0	0
Outlet 3	0.005	−0.001	0

rate at the outputs decreases. Comparing the time cost being spent on the numerical calculations for each grid, in the case of calculations in a model with rigid walls, calculations on grids of 1 million elements were carried out within 10 minutes, while calculations on a grid of 8 million elements took more than an hour for the same Core i7 PC. Considering FSI models, the difference in time cost was large with minor changes in the result. Thus, we can say that a grid consisting of 1 million elements for such calculations is optimal, therefore such grids are used for all calculations in this study.

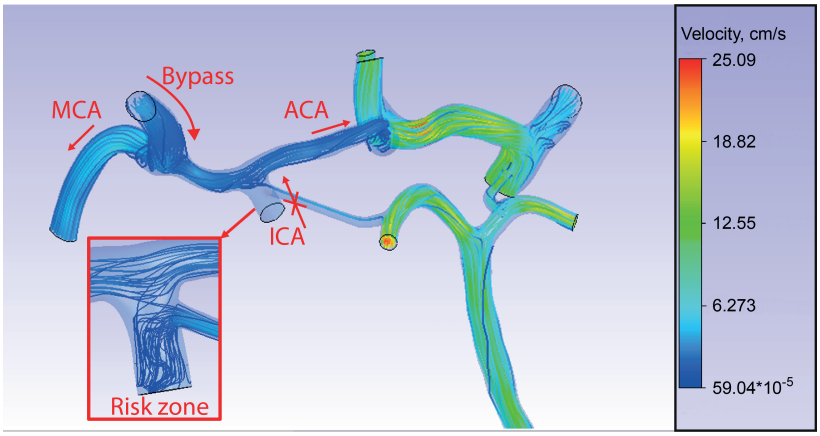

Figure 3. The stagnant zone is found at the rest compartment (risk zone) of ICA after the clipping. The enlarged image shows the trajectories of particles launched inside this region, i.e., particles trapped in a formed vortex. The highlighted area does not contain the particles that started from the left ICA inlet.

1.6. Methodology of the numerical simulations

In this study, we presume that the hydrodynamic features of the entire cerebral vasculature can affect the outcome of a bypass installation, which significantly expands assumption used in [19]. Taking this into account, it is necessary to analyze a certain general indicator related to the entire vasculature. We found that when solving the model problem of the optimal angle of anastomosis [17], this parameter can be the value of the viscous dissipation of blood flow energy in the circulation domain. The same indicator was chosen in the current work. The equation of viscous dissipation of energy for domain Ω per 1 sec is defined [28] as follows:

$$D = \int_{\Omega} |\omega^2| \, \mathrm{d}\Omega \tag{1.7}$$

where ω is a vorticity.

The indicated value determines the amount of energy that is dissipated in the blood flow as it passes through the vascular network. This energy can be directed to: deformation of the vessel wall or to maintain vortices in the domain, stagnant zones as subdomains of cerebral circulation (see Fig. 3), the presence of which [13, 39] can lead to thrombosis. However, it is obvious that such a value substantially depends on the volume (the energy dissipated in the system grows with the growing volume) of the domain and for the correct comparison of the data from different patients, it is necessary to consider an indicator that is independent of their cerebral circulation domain volume. As such an indicator, we have chosen the value of the specific energy dissipation equal to:

$$D_{\text{unit}} = \left(\int_{\Omega} |\omega^2| \, \mathrm{d}\Omega \right) / |\Omega| \tag{1.8}$$

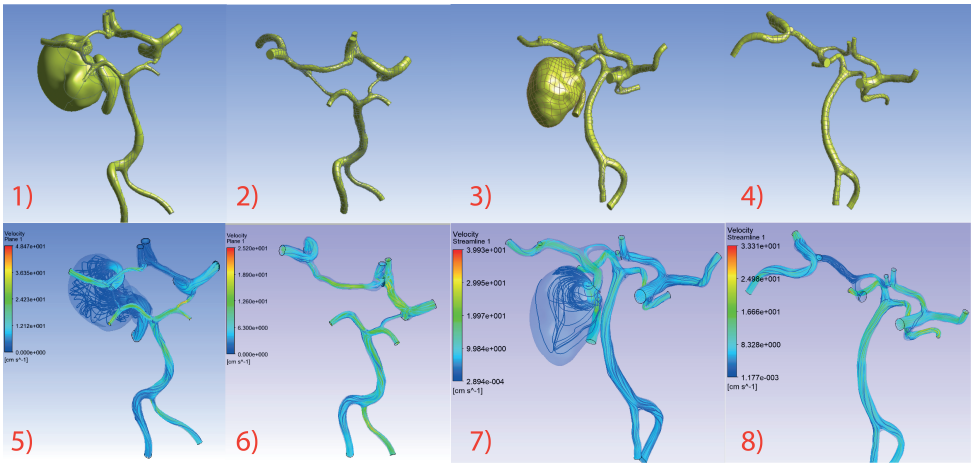

Figure 4. 1) Geometry of the COW for Patient A before the treatment; 2) Geometry of the COW for Patient A with bypass formed after aneurysm occlusion; 3) Geometry of the COW for Patient B (rotated 180 degrees) before the treatment; 4) Geometry of the COW for Case B (rotated 180 degrees) after the treatment; 5) Velocity streamlines for Patient A before the treatment; 6) Velocity streamlines Patient A after the treatment and aneurysm occlusion; 7) Velocity streamlines for Patient B (rotated 180 degrees) before the treatment; 8) Velocity streamlines for Patient B (rotated 180 degrees) after the treatment. For Patient B rotated 180 degrees configuration is presented to better understand a little difference between configurations in volume and quantity of reconstructed configuration.

where $|\Omega|$ is the volume of a computational domain Ω. From the point of view of both the efficiency of the circulatory network and its safety, this value should be minimal. The growth of this energy increases the loss of blood flow energy in the COW. Consequently, the pressure in the distal sections of the vascular network drops, which can lead to its transport failure.

2. Results

Numerical simulations were performed in ANSYS 17.2 (CFX+Structural). In Fig. 4 the stagnant zone is not visible, since a limited number of the streamlines were specified during the construction of streamlines and, due to extremely low velocities, the flow was not visualized in this region. To visualize a streamlines in a stagnant zone, it was necessary to specify additional starting points for streamlines near this zone. The established fact indicates the difficulty of detecting such a zone of stagnation both numerically and when observing a patient in a hospital.

As a result of numerical simulation, the hemodynamics parameters, such as viscous dissipation energy and flow rate, were calculated (see Tables 3–5). It was found that for both patients there was an increase in the specific energy of viscous dissipation per 1 sec (D_{unit}), moreover, this growth was more significant for virtual surgery than for an alternative treatment technique, which indirectly indicates the correctness of the decision to impose an anastomosis for both cases. It turned out that the hydrodynamic system of cerebral vessels has become less effective than before the anastomosis was formed, but more effective than the virtual alternative technique.

Table 3. The values of principle hemodynamic quantities in the steady case of the configuration with rigid walls before and after surgery and assuming that the shunt was not installed.

	AcomA cross-sectional area (cm^2)	Q through AComA (g/s)	D value (J/s) $\times 10^{-7}$	V (cm^3)	D_{unit} ($J/cm^{-3}s$) $\times 10^{-7}$	D value (J/s) $\times 10^{-7}$	V (cm^3)	D_{unit} ($J/cm^{-3}s$) $\times 10^{-7}$
				Case A				
before	0.30	0.33	45293.4	92.37	490.38	35017.5	12.74	2749.51
after	0.64	3.40	15574.6	21.18	735.51	—	—	—
without shunt	0.58	3.25	21433.4	17.63	1215.81	—	—	—
				Case B				
before	0.36	0.11	28631.6	90.72	315.59	25045.8	18.47	1355.73
after	0.23	0.95	27552.3	17.33	1589.76	—	—	—
without shunt	0.24	0.97	25230.3	14.46	1744.72	—	—	—
	Full model (healthy compartment + aneurysm volume)					Healthy compartment		

Table 4. The values of principle hemodynamic quantities in the steady case of the configuration with FSI before and after surgery and assuming that the shunt was not installed.

	AcomA cross-sectional area (cm^2)	Q through AComA (g/s)	D value (J/s) $\times 10^{-7}$	V (cm^3)	D_{unit} ($J/cm^{-3}s$) $\times 10^{-7}$	D value (J/s) $\times 10^{-7}$	V (cm^3)	D_{unit} ($J/cm^{-3}s$) $\times 10^{-7}$
				Case A				
before	0.29	0.3	46074.3	92.40	498.67	44814.5	13.58	3299.68
after	0.65	3.46	22980.2	21.18	1085.2	—	—	—
without shunt	0.65	3.49	22185.2	17.63	1258.41	—	—	—
				Case B				
before	0.34	0.12	33090.2	90.82	364.37	27679	18.48	1498.13
after	0.23	1.13	31715.7	17.33	1829.91	—	—	—
without shunt	0.24	1.18	30507.4	14.46	2109.57	—	—	—
	Full model (healthy compartment + aneurysm volume)					Healthy compartment		

Table 5. The values of principle hemodynamic quantities in the transient case of the configuration with rigid walls before and after surgery and assuming that the shunt was not installed.

	AcomA cross-sectional area (cm^2)	Q through AComA (g/s)	D value (J/s) $\times 10^{-7}$	V (cm^3)	D_{unit} ($J/cm^{-3}s$) $\times 10^{-7}$	D value (J/s) $\times 10^{-7}$	V (cm^3)	D_{unit} ($J/cm^{-3}s$) $\times 10^{-7}$
				Case A				
before	0.30	0.28	42578.8	92.36	474.97	42578.82	13.58	3135.38
after	0.64	3.13	21164.9	21.18	999.51	—	—	—
without shunt	0.58	2.87	18486.1	17.63	1048.62	—	—	—
				Case B				
before	0.36	0.18	29246.5	90.72	347.31	26010.8	18.47	1407.97
after	0.23	1.04	28814.8	17.33	1662.60	—	—	—
without shunt	0.24	1.08	27523.2	14.46	1903.28	—	—	—
	Full model (healthy compartment + aneurysm volume)					Healthy compartment		

Table 6. The values of pressure in the MCA before operation (iMCAP), at the moment of the occlusion during the operation and $\mathrm{MCAP}_{\mathrm{ratio}}$ for both patients.

	iMCAP	cMCAP	r_{graft}	r_{ICA}	$\mathrm{MCAP}_{\mathrm{ratio}}$
Patient A	90.18	90.1	7.14	6.75	0.98
Patient B	90.20	89.9	4.99	7.17	0.99

Despite the fact that, from the point of view of hydrodynamics, the system has become slightly less efficient, however, by eliminating the aneurysm from the circulation, the risk of its rupture was eliminated. Comparing the results of simulation for rigid case and FSI approach, we noted that the qualitative changes are the same for both approaches. It is not correct to quantify these approaches, since for FSI calculation the blood flow deflects the wall, which changes both the volume and the geometry of the blood flow domain.

For all approaches used: steady, FSI and non-stationary, there is a significant difference in the D_{unit} value calculated for the *healthy compartment* for the cases with (Patient A) and without (Patient B) complications.

In the case of stationary formulation for Patient A the value of D_{unit} is 2.2 times higher than the same value for Patient B in the FSI model before operation in healthy compartment and 2.02 times higher in the configuration with rigid walls. At the same time in the full model (healthy compartment + aneurysm volume) for Patient A this value is 1.37 times higher in the FSI model and 1.55 times higher in the configuration with rigid walls (see Tables 3 and 4).

In the case of transient formulation, we noted qualitatively the same relations between D_{unit} in the case of calculation for a network of vessels for patients with and without complication, as in a stationary setting. This result is quite expected since $w = \mathrm{rot}\,(v)$, and thus, the desired integral will be a function of the volumetric blood flow. A similar fact has already been noted in [9]: for the purpose of calculating volumetric blood flow, taking into account the pulsating nature of the blood flow does not give significantly more accurate results compared to a stationary calculation that uses averaged data to set the boundary conditions in the computational fluid domain.

3. Discussion

The motivation for this study was appeared after analyzing the approach described in [19] in relation to the described clinical cases. Namely, the calculation of parameters that are based on the geometry of the vascular domain and are described by the formula:

$$\mathrm{MCAP}_{\mathrm{ratio}} = (1-k)\left(\frac{r_{\mathrm{graft}}}{r_{\mathrm{ICA}}}\right)^2 + k \tag{3.1}$$

we obtained that coefficient $r_{\mathrm{graft}}/r_{\mathrm{ICA}} = 3.57/3.375$, and as a final value MCAP ratio ¿ 0.8 (see Table 6), that according to [19] means a good quality of bypass function. The inferiority of the criterion is due to the fact that it does not take into

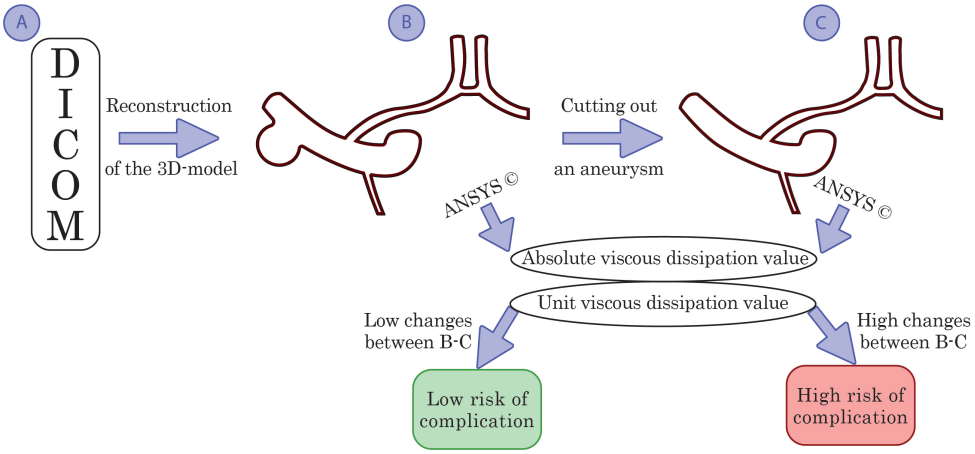

Figure 5. Roadmap of the study: from DICOM images towards dissipative reserve calculation.

account either the flow of blood throughout the network, the features of its geometry, interaction of the blood flow with the wall, pulsating nature of the blood flow. This example shows the insufficiency of the parameter available in the literature for the correct adoption of a medical decision.

The parameter we use shows both qualitative and quantitative changes in the hydrodynamics of the cerebral vascular network. Previously, it has already shown its effectiveness in the model problem of the optimal angle of the bypass installation [17] and in the validation of the rupture risk of multiple cerebral aneurysms [16].

From the results (see Tables 3–5) we see that by the value of parameter D_{unit} (for healthy compartment) one can qualitatively judge the initial tendency of cerebral vasculature for appearing clots. Its higher value, means the higher dissipative characteristics of the COW and, as a consequence, the lower its efficiency. Thus, parameter D_{unit} for healthy domain (as we call it 'dissipative reserve') can be considered as a new indicator for increased attention to the patient in some cases like bypass installing.

In addition, the results of the study show that the complication of the calculation model is impractical, because a qualitative result is preserved for all used approaches. The proposed scheme of the used approach is shown in Fig 5.

A limitation of this study is a small sample of patients. At the moment, we only qualitatively understand the differences in the case with and without complication. The purpose of further research will be to calculate the dissipative reserve for amount of patients accumulate statistical information to form a quantitative criterion that allows to determine the boundary of the zone of occurrence of possible complications. Moreover, we used simple Newtonian approach as blood viscosity model. In some papers it was shown that the viscosity model significantly changes hemodynamic of domain with stagnant zones like aneurysms. However, as noted above, the approach should not be complicated if it works well.

4. Conclusion

A new qualitative criterion is proposed for assessing risk of prescribed events of blood clots during revascularization procedures in cerebral blood vessels. The criterion takes into account the geometry of cerebral vasculature and is based on the optimization of the unit energy of viscous dissipation per 1 sec, which characterizes the effectiveness of cerebral vessels as a hydrodynamic system. Considering that additional cases could provide quantitative criterion of postoperative complications for cerebral shunting procedures.

Abbreviations

AComA — anterior communicating artery
COW — circle of Willis
CT — computed tomography
EC-IC bypass — extracranial–intracranial bypass
FSI — fluid–solid interface
IA — intracranial aneurysms
ICA — internal carotid artery
M1 — segment of middle cerebral artery
MCA — middle cerebral artery
MCAP — middle cerebral artery pressure
TA — temporal artery
VA — vertebral artery
WSS — wall shear stress

References

1. O. Baskurt, M. Hardeman, M. Rampling, and H. Meiselman, *Handbook of Hemorheology and Hemodynamics. Biomedical and Health Research*, IOS Press, 2007.

2. J. Boyd, J. Buick, and S. Green, Analysis of the Casson and Carreau–Yasuda non-Newtonian blood models in steady and oscillatory flows using the lattice Boltzmann method. *Physics of Fluids* **19** (2007), No. 9.

3. I. Campbell, L. Timmins, D. Giddens, R. Virmani, A. Veneziani, S. Rab, H. Samady, M. McDaniel, A. Finn, W. Taylor, and J. Oshinski, Computational fluid dynamics simulations of hemodynamics in plaque erosion. *Cardiovascular Engineering and Technology* **4** (2013), No. 4, 464–473.

4. O. Choudhri, N. Mukerji, and G. Steinberg, Combined endovascular and microsurgical management of complex cerebral aneurysms. *Frontiers in Neurology* **4** (2013), 108.

5. J. Davies and M. Lawton, Advances in open microsurgery for cerebral aneurysms. *Neurosurgery* **74** (Supplement 1) (2014), S7–S16.

6. I. Despotovi, B. Goossens, and W. Philips, MRI segmentation of the human brain: Challenges, methods, and applications. *Computational and Mathematical Methods in Medicine* (2015), No. 1, 450341.

7. G. Esposito, J. Fierstra, and L. Regli, *Partial Trapping Strategies for Managing Complex Intracranial Aneurysms*. Springer International Publishing, 2016.

8. G. Esposito, M. Sebk, S. Amin-Hanjani, and L. Regli, Cerebral bypass surgery: level of evidence and grade of recommendation. In: *Trends in the Management of Cerebrovascular Diseases*, Springer, 2018, pp. 73–77.

9. A. Geers, I. Larrabide, H. Morales, and A. Frangi, Approximating hemodynamics of cerebral aneurysms with steady flow simulations *Journal of Biomechanics* **47** (2014), No. 1, 178–185.

10. D. Griswold, A. Benet, H. Tabani, M. Lawton, and A. Meybodi, 'To operate' versus 'not to operate' in low-resource settings: Example of aneurysm surgery in rural iran and impact of mastery of neurosurgical anatomy. *World Neurosurgery* **100** (2017), 628–631.

11. B. Grter, I. Mendelowitsch, M. Diepers, L. Remonda, J. Fandino, and S. Marbacher, Combined endovascular and microsurgical treatment of arteriovenous malformations in the hybrid operating room. *World Neurosurgery* **117** (2018), e204e214.

12. O. Hajati, K. Zarrabi, R. Karimi, and A. Hajati, CFD simulation of hemodynamics in sequential and individual coronary bypass grafts based on multislice ct scan datasets. In: *2012 Annual International Conference of the IEEE Engineering in Medicine and Biology Society*. IEEE, 2012, pp. 641–644.

13. J. Hathcock, Flow effects on coagulation and thrombosis, Arteriosclerosis. *Thrombosis, and Vascular Biology* **26** (2006), No. 8, 1729–1737.

14. What is an aneurysm? American association of neurological surgeons. http://www.aans.org/patients/neurosurgical-conditions-and-treatments/cerebral-aneurysm.

15. L. Kivipelto, M. Niemel, T. Meling, M. Lehecka, H. Lehto, and J. Hernesniemi, Bypass surgery for complex middle cerebral artery aneurysms: Impact of the exact location in the MCA tree: Clinical article. *Journal of Neurosurgery* **120** (2014), No. 2, 398–408.

16. A. Khe, A. Chupakhin, A. Cherevko, S. Eliava, and Y. Pilipenko, Viscous dissipation energy as a risk factor in multiple cerebral aneurysms. *Russian Journal of Numerical Analysis and Mathematical Modelling* **30** (2015), No. 5, 277–287.

17. Y. Kuyanova, S. Presnyakov, A. Dubovoi, A. Chupakhin, and D. Parshin, Numerical study of the tee hydrodynamics in the model problem of optimizing the low-flow vascular bypass angle. *Journal of Applied Mechanics and Technical Physics* **60** (2019), No. 6, 1038–1045.

18. S. Maltseva, A. Cherevko, A. Khe, A. Akulov, A. Savelov, A. Tulupov, E. Derevtsov, M. Moshkin, and A. Chupakhin, Reconstruction of complex vasculature by varying the slope of the scan plane in high-field magnetic resonance imaging. *Applied Magnetic Resonance* **47** (2015), No. 1, 23–39.

19. H. Matsukawa, S. Miyata, T. Tsuboi, K. Noda, N. Ota, O. Takahashi, R. Takeda, S. Tokuda, H. Kamiyama, and R. Tanikawa, Rationale for graft selection in patients with complex internal carotid artery aneurysms treated with extracranial to intracranial high-flow bypass and therapeutic internal carotid artery occlusion. *Journal of Neurosurgery* **128** (2018), No. 6, 1753–1761.

20. H. Matsukawa, R. Tanikawa, H. Kamiyama, T. Tsuboi, K. Noda, N. Ota, S. Miyata, R. Takeda, and S. Tokuda, Graft occlusion and graft size changes in complex internal carotid artery aneurysm treated by extracranial to intracranial bypass using high-flow grafts with therapeutic internal carotid artery occlusion. *Neurosurgery* **81** (2017), No. 4, 672–679.

21. K. Matsuura, W. Jin, H. Liu, and G. Matsumiya, Computational fluid dynamic study of different incision length of coronary artery bypass grafting in a native coronary stenosis model. *Journal of Thoracic Disease* **11** (2019), No. 2, 393–399.

22. D. Parshin, Y. Kuyanova, D. Kislitsin, U. Windberger, and A. Chupakhin, On the impact of flow-diverters on the hemodynamics of human cerebral aneurysms. *Journal of Applied Mechanics and Technical Physics* **59** (2018), No. 6, 963–970.

23. L. Pierot and A. Wakhloo, Endovascular treatment of intracranial aneurysms: Current status. *Stroke* **44** (2013), No. 7, 2046–2054.

24. G. Rinkel, M. Djibuti, A. Algra, and J. van Gijn, Prevalence and risk of rupture of intracranial aneurysms: A systematic review. *Stroke* **29** (1998), No. 1, 251–256.

25. J. Russin, H. Babiker, J. Ryan, L. Rangel-Castilla, D. Frakes, and P. Nakaji, Computational fluid dynamics to evaluate the management of a giant internal carotid artery aneurysm. *World Neurosurgery* **83** (2015), No. 6, 1057–1065.

26. L. Sekhar, S. Natarajan, R. Ellenbogen, and B. Ghodke, Cerebral revascularization for ischemia, aneurysms, and cranial base tumors. *Neurosurgery* **62** (2008), No. 6, SHC1373SHC1410.

27. S. Sia, Y. Qian, W. Matsuda, A. Avolio, and M. Morgan, *Evaluation of Brain Extracranial-to-Intracranial (EC-IC) Bypass Treatments by Using Computational Hemodynamic Technology*. Springer, Berlin–Heidelberg, 2010.

28. N. Slyozkin, *Dynamics of Viscous Incompressible Fluid*. GITTL, 1955.

29. I. Tagiltsev, D. Parshin, and A. Shutov, Rational choice of modelling assumptions for simulation of blood vessel end-to-side anastomosis. *Mathematical Modelling of Natural Phenomena* **17** (2022), 20.

30. S. Thanapal, S. Duvuru, T. Sae-Ngow, Y. Kato, and K. Takizawa, Direct cerebral revascularization: Extracranial-intracranial bypass. *Asian Journal of Neurosurgery* **13** (2018), No. 1, 9–17.

31. G. Toth and R. Cerejo, Intracranial aneurysms: Review of current science and management. *Vascular Medicine* **23** (2018), No. 3, 276–288.

32. B. Walcott, C. Reinshagen, C. Stapleton, O. Choudhri, V. Rayz, D. Saloner, and M. Lawton, Predictive modeling and invivo assessment of cerebral blood flow in the management of complex cerebral aneurysms. *Journal of Cerebral Blood Flow & Metabolism* **36** (2016), No. 6, 998–1003.

33. P. Yushkevich, J. Piven, H. Hazlett, R. Smith, S. Ho, J. Gee, and G. Gerig, User-guided 3D active contour segmentation of anatomical structures: Significantly improved efficiency and reliability. *NeuroImage* **31** (2006), No. 3, 1116–1128.

34. L. Zarrinkoob, K. Ambarki, A. Whlin, R. Birgander, A. Eklund, and J. Malm, Blood flow distribution in cerebral arteries. *Journal of Cerebral Blood Flow & Metabolism* **35** (2015), No. 4, 648–654.

35. H. Zhang, T. Schneider, C. Wheeler-Kingshott, and D. Alexander, Noddi: Practical in vivo neurite orientation dispersion and density imaging of the human brain. *NeuroImage* **61** (2012), No. 4, 1000–1016.

36. M. Zhang, F. Peng, Y. Li, L. He, A. Liu, and R. Li, Associations between morphology and hemodynamics of intracranial aneurysms based on 4D flow and black-blood magnetic resonance imaging. *Quantitative Imaging in Medicine and Surgery* **11** (2021), No. 2, 597–607.

37. F. Zhu, Y. Qian, B. Xu, Y. Gu, K. Karunanithi, W. Zhu, L. Chen, Y. Mao, and M. Morgan, Quantitative assessment of changes in hemodynamics of the internal carotid artery after bypass surgery for moyamoya disease. *Journal of Neurosurgery* **129** (2018), No. 3, 677–683.

38. F.-P. Zhu, Y. Zhang, M. Higurashi, B. Xu, Y.-X. Gu, Y. Mao, M. Morgan, and Y. Qian, Haemodynamic analysis of vessel remodelling in STA-MCA bypass for moyamoya disease and its impact on bypass patency. *Journal of Biomechanics* **47** (2014), No. 8, 1800–1805.

39. J. Zilberman-Rudenko, J. Sylman, H. Lakshmanan, O. McCarty, and J. Maddala, Dynamics of blood flow and thrombus formation in a multi-bypass microfluidic ladder network. *Cellular and Molecular Bioengineering* **10** (2016), No. 1, 16–29.